

pubs.acs.org/JACS Article

What Is the Rate-Limiting Step of Oxygen Reduction Reaction on Fe-N-C Catalysts?

Saerom Yu, Zachary Levell, Zhou Jiang, Xunhua Zhao, and Yuanyue Liu*



Cite This: J. Am. Chem. Soc. 2023, 145, 25352-25356



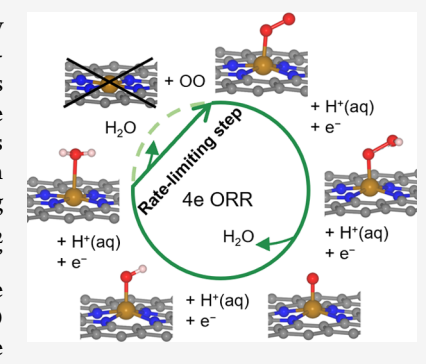
ACCESS

III Metrics & More

Article Recommendations

Supporting Information

ABSTRACT: Oxygen reduction reaction (ORR) is essential to various renewable energy technologies. An important catalyst for ORR is single iron atoms embedded in nitrogendoped graphene (Fe–N–C). However, the rate-limiting step of the ORR on Fe–N–C is unknown, significantly impeding understanding and improvement. Here, we report the activation energies of all of the steps, calculated by ab initio molecular dynamics simulations under constant electrode potential. In contrast to the common belief that a hydrogenation step limits the reaction rate, we find that the rate-limiting step is oxygen molecule replacing adsorbed water on Fe. This occurs through concerted motion of H_2O desorption and O_2 adsorption, without leaving the site bare. Interestingly, despite being an apparent "thermal" process that is often considered to be potential-independent, the barrier reduces with the electrode potential. This can be explained by stronger Fe– O_2 binding and weaker Fe– H_2O binding at a lower potential, due to O_2 gaining electrons and H_2O donating electrons to the



catalyst. Our study offers new insights into the ORR on Fe-N-C and highlights the importance of kinetic studies in heterogeneous electrochemistry.

■ INTRODUCTION

Oxygen reduction reaction (ORR) is essential to a variety of renewable energy technologies such as fuel cells and metal—air batteries. Platinum is the best-performing catalyst for ORR. However, it suffers from high cost, which impedes its commercial use. To overcome this obstacle, tremendous research efforts have been dedicated to finding cost-effective alternative catalysts to Pt. One of the most promising candidates is single iron atoms embedded in nitrogen-doped graphene (Fe-N-C), which is often used in acidic conditions. Despite extensive studies on this catalyst, it is still unknown what step limits the ORR rate on Fe-N-C. The lack of this critical information significantly limits catalyst development.

A commonly suggested pathway for ORR on Fe-N-C has the following steps (Figure 1a): * + $O_2 \rightarrow *OO$, * $OO + H^+ +$ $e^{-} \rightarrow *OOH, *OOH + H^{+} + e^{-} \rightarrow *O + H_{2}O, *O + H^{+} + e^{-}$ \rightarrow *OH, *OH + H⁺ + e⁻ \rightarrow * + H₂O. Experimental determination of the rate-limiting step is challenging. On the other hand, density functional theory (DFT) offers a means to calculate the reaction energetics, including activation energies, and thus in principle can answer the question about the rateliming step. However, directly calculating activation energies of heterogeneous electrochemistry is difficult due to the complexity of the system, which requires careful treatments of the effects of solvation and electrode potential. 19-29 Therefore, most computational studies calculate the thermodynamics of each step and use it to infer the kinetics, based on the assumption that the most thermodynamically uphill (or the least downhill) step has the highest activation energy. Those

papers typically show that either the *OO + H $^+$ + e $^ \rightarrow$ *OOH or the *OH + H $^+$ + e $^ \rightarrow$ * + H $_2$ O step is the thermodynamically limiting step. ^{29–36} Both steps involve hydrogenation of the adsorbate. However, thermodynamics does not necessarily correlate with kinetics. Hence, the information on activation energies is indispensable to identify the rate-limiting step.

To address this critical need, here we calculate the activation energies of ORR steps on Fe–N–C, using a recently developed model: "constant-potential hybrid solvation-dynamic model" (CP-HS-DM). This model enables effective simulation of electrochemical kinetics at the solid—water interface, by directly including the explicit solvation and electrode potential into the model. The results reveal a different reaction mechanism from the commonly believed one: instead of the hydrogenation step, the rate-limiting step is the replacement of the preadsorbed $\rm H_2O$ molecule by the $\rm O_2$ molecule on the Fe atom; despite being an apparent "thermal" process, the activation energy of this step decreases with decreasing electrode potential, due to the enhanced $\rm Fe-O_2$ binding while weakened $\rm Fe-OH_2$ binding at a lower potential. Our work provides new insights into the ORR and $\rm Fe-N-C$

Received: August 22, 2023
Revised: October 17, 2023
Accepted: October 26, 2023
Published: November 13, 2023





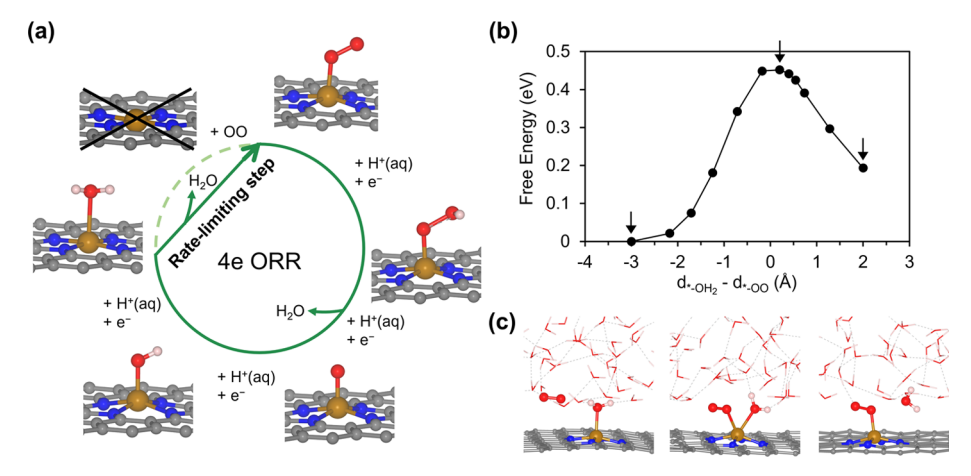


Figure 1. (a) Schematic illustration of the ORR mechanism. (b) Free energy profile of $*H_2O + O_2 \rightarrow *O_2 + H_2O$ at 0.5 V vs SHE. (c) Representative structures chosen from the reaction coordinate values marked by arrows. Brown, blue, gray, red, and white spheres represent iron, nitrogen, carbon, oxygen, and hydrogen atoms, respectively.

catalytic mechanisms and highlights the significance of kinetic information that is generally lacking in the current study of heterogeneous electrocatalysis.

METHODS

The CP-HS-DM²⁰ is one realization of the constant-potential ab initio molecular dynamics (cp-AIMD) with explicit water. The supercell contains a thin film of explicit water molecules on top of the catalyst. The remaining space is filled with implicit solution modeled as a continuous dielectric medium with point ionic charges. This implicit solution serves to balance the extra charges in the explicit region and introduces a region with a flat electrostatic potential profile that can be used to extract the relative electrode potential. The structure is evolved using AIMD with an enhanced sampling technique, and the electron number changes under potentiostat.

In this work, we perform CP-HS-DM simulation using Vienna Ab initio Simulation Package (VASP),^{37,38} leveraging the VASPsol^{39,40} implicit solvation model. We have implemented the cp-AIMD method as a patch to the VASP code (the patch file is available to the readers upon reasonable request). To compute the free energy profile, we employed thermodynamic integration. Specifically, we first run slow-growth simulation⁴¹ to obtain a preliminary profile and then run blue moon simulation^{42,43} to obtain a more accurate one. To model the acidic conditions, we add one H to the explicit water molecules. The details of our calculations can be found in the Supporting Information (SI).

RESULTS AND DISCUSSION

Our study first focuses on U = 0.5 V vs SHE because it is within the typical range of working potentials. ^{12,44,45} Our cp-AIMD simulations show that when Fe-N-C is in contact with water, a $\rm H_2O$ molecule is adsorbed onto the Fe site. When we intentionally desorb $\rm H_2O$ via slow growth, another $\rm H_2O$ molecule will occupy the Fe site (see SI Section 3). This result indicates that before ORR, the Fe site is already occupied by a $\rm H_2O$ molecule, consistent with a recent paper. ²⁹

Then how does the adsorption of O_2 take place? We find that the adsorption of O_2 occurs concertedly with H_2O desorption. As shown in Figure 1c, as the O_2 in the solvent approaches the Fe to form the Fe–OO bond, it displaces the adsorbed H_2O to break the Fe–OH $_2$ bond. Eventually, the O_2 replaces the H_2O and becomes adsorbed on the Fe. During this process, the Fe atom remains bonded with the adsorbate(s) (either H_2O or O_2 or both), which lowers the energy cost and results in a barrier of 0.45 eV, as shown in

Figure 1b. Particularly, at the transition state, both H_2O and O_2 are bonded to the Fe site. These results suggest a different reaction mechanism from the commonly accepted one: the steps $^*H_2O \rightarrow ^* + H_2O$ and $O_2 + ^* \rightarrow ^*OO$ steps are not separate; instead, they occur simultaneously and thus should be written together as $^*H_2O + O_2 \rightarrow ^*O_2 + H_2O$ (Figure 1a).

We further study the subsequent steps, i.e., $*OO + H^+ + e^- \rightarrow *OOH$, $*OOH + H^+ + e^- \rightarrow *O + H_2O$, $*O + H^+ + e^- \rightarrow *OH$, and $*OH + H^+ + e^- \rightarrow *OH_2$. These are electrochemical steps. Figure 2 shows the $*OOH + H^+ + e^- \rightarrow *O + OOH$

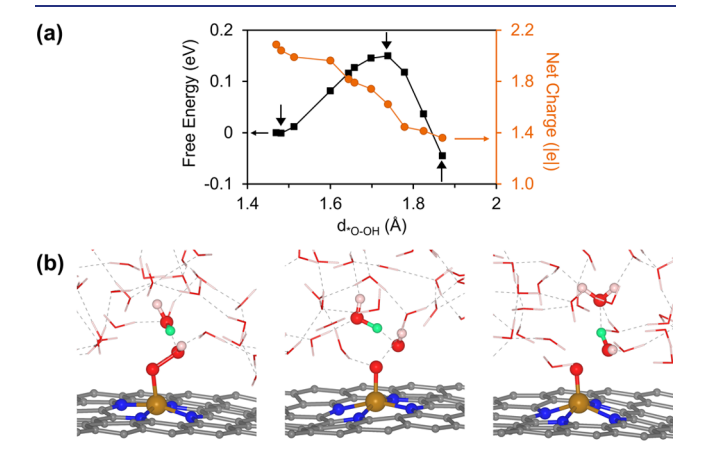


Figure 2. (a) *OOH + H⁺ + e⁻ \rightarrow *O + H₂O free energy profile and net charge evolution at U = 0.5 V vs SHE. (b) Representative structures chosen from the reaction coordinate values marked by arrows. The proton transferred to *OOH is highlighted in green.

 $\rm H_2O$ step as an example. In this step, as the *O-OH bond breaks, the proton attacks the generated OH to form $\rm H_2O$. During this process, the system gradually acquires excessive electron concentrating on the higher O, which attracts the proton closer and facilitates the $\rm H_2O$ formation. Consequently, the barrier is low, only 0.15 eV. It is worth noting that this change in electron number cannot be observed in the conventional constant-charge simulation, thereby necessitating the use of the constant-potential method as we employed here. Additionally, the Fe-N-C surface exhibits a positive charge under 0.5 V. This is because its potential of zero charge (PZC) is lower than 0.5 V. In other words, at a charge-neutral state,

the Fermi level of Fe–N–C is higher than that of the electrode. To align the Fermi levels, Fe–N–C has to lose electrons, thereby acquiring a positive charge. Another interesting finding is that at the initial state, the proton is located closer to the higher O than the lower O in the *O–OH on Fe–N–C. This contrasts the Co–N–C catalyst, where the proton prefers the lower O. Therefore, after the proton attacks the closer O, Fe–N–C will generate H_2O , whereas Co–N–C will produce H_2O_2 . This explains the difference in ORR selectivity observed for these two catalysts.

Figure 3 provides a comprehensive summary of the energy barriers for all ORR steps. Note that the *O + H $^+$ + e $^ \rightarrow$

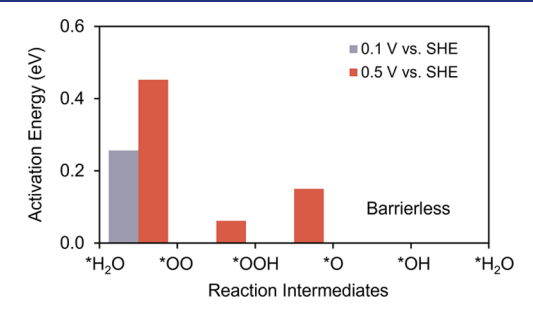


Figure 3. Energy barriers for all of the ORR steps under different potentials.

*OH and *OH + H⁺ + e⁻ \rightarrow *OH₂ steps do not have barriers because in our simulations (without geometric constraint), the protons spontaneously diffuse to the adsorbates, completing the steps (see SI Section 5). The comparison shows that the *H₂O + O₂ \rightarrow *O₂ + H₂O step has the highest activation energy and is thus the rate-limiting step. This finding contrasts the common belief based on thermodynamic considerations that the hydrogenation step is rate-limiting.

To check if our conclusion still holds at a lower potential, we also study ORR at U=0.1 V vs SHE. This potential is chosen because it is not too low to be unrealistic but low enough to show a significant difference. ^{12,44,45} As shown in Figure 3, we find that all electrochemical steps become barrierless while the *H₂O + O₂ \rightarrow *O₂ + H₂O step still has a barrier of 0.26 eV. Therefore, the rate-limiting step is still *H₂O + O₂ \rightarrow *O₂ + H₂O.

It is interesting to see that the activation energy of ${}^*H_2O + O_2 \rightarrow {}^*O_2 + H_2O$ noticeably decreases when the potential is decreased (Figure 3). This challenges the conventional view that it is a thermal step (as it does not explicitly involve electron(s)) and should be potential-independent. To understand the origin, we calculate the adsorption energies of O_2 and H_2O on Fe-N-C under different potentials (without solvent molecules for simplicity). As shown in Figure 4a, decreasing

the potential enhances the O_2 adsorption while weakening the H_2O adsorption. Therefore, the lower barrier at the lower potential can be explained by the stronger driving force provided by the enhanced binding with O_2 and the weakened binding with H_2O .

The potential-induced change in the binding strength can be attributed to different surface charges under different potentials. Our calculations (without solvent for simplicity) show that the bare Fe-N-C acquires ~1 electron as the potential decreases from 0.5 to 0.1 V. This large change in the surface charge results in a significant change in the electronic state occupation, thereby altering the chemical reactivity of Fe-N-C. 21 But why do O_2 and H_2O have opposite responses to the surface charge? This can be explained by the opposite directions of charge transfer. We find that upon adsorption, O2 gains electrons from Fe-N-C while H2O donates electrons (see Figure 4b). Increasing the electronic charges on Fe-N-C will enhance the electron transfer to the adsorbate while suppressing the back-transfer. Therefore, reducing the potential strengthens the binding with O2 while weakening that with H2O. This mechanism suggests that to design more active sites for ORR, one may target those that are more negatively charged (under the same electrode potential), because they can have lower activation energies for the ratelimiting step of $*H_2O + O_2 \rightarrow *O_2 + H_2O$.

The charge transfer theory also explains the potential dependence of the adsorption energies of other intermediates (*OOH, *O, and *OH). As shown in Figure S9a, the potential decrease enhances their bindings with the catalyst. This can be attributed to the fact that they all gain electrons from the catalyst (Figure S9b).

Although our focus here is on the acidic conditions, as Fe–N–C is mainly used in proton exchange member fuel cells, it is worth considering other pH conditions. For the same RHE potential, the SHE potentials are lower under alkaline conditions than under acid conditions. In other words, the catalyst surface is more negatively charged under alkaline conditions. According to our findings, a more negatively charged site should have a lower barrier for the *H₂O + O₂ \rightarrow *O₂ + H₂O step. On the other hand, the proton source is a water molecule under alkaline conditions and it is more difficult to donate protons than H₃O⁺. Therefore, compared with acidic conditions, we anticipate that in alkaline conditions the *H₂O + O₂ \rightarrow *O₂ + H₂O step will become easier, whereas the hydrogenation steps will become more difficult.

CONCLUSIONS

In this study, we employed an advanced first-principles model to reveal the rate-limiting step of ORR on Fe-N-C. We discovered a new mechanism that O_2 replaces the preadsorbed

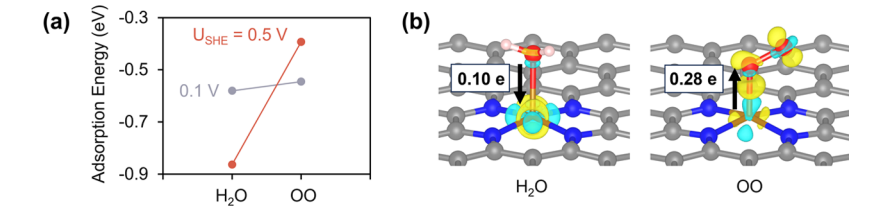


Figure 4. (a) Adsorption energies of H_2O and O_2 on Fe-N-C under different potentials. (b) Isosurfaces of the electronic density change due to the adsorptions. Yellow represents electron accumulation, and cyan represents electron depletion (isovalue = 0.015 e Å⁻³). The black arrows indicate the directions of the electron transfer, and the numbers show the magnitude of charge transfer using the Bader partition method.

H₂O on Fe through a concerted motion without leaving the Fe site bare. This step was found to have the largest activation energy among the ORR steps. The barrier of this step counterintuitively lowers with decreasing electrode potential, due to the stronger O2 adsorption and weaker H2O adsorption when the surface carries more electronic charges. This can be further explained by the fact that O₂ adsorption gains electrons from the surface while H₂O donates electrons to the surface. These results suggest that a more negatively charged site would be more active for the ORR. Our work emphasizes the importance of kinetic information in understanding and designing heterogeneous electrocatalysts.

ASSOCIATED CONTENT

Supporting Information

The Supporting Information is available free of charge at https://pubs.acs.org/doi/10.1021/jacs.3c09193.

> General settings of DFT calculations; details of electronic charge calculation; structure evolution for water adsorption dynamics; details of energy barrier calculations; more reaction kinetics data; and adsorption energies and electronic charge transfer of ORR intermediates (PDF)

AUTHOR INFORMATION

Corresponding Author

Yuanyue Liu - Texas Materials Institute and Department of Mechanical Engineering, The University of Texas at Austin, Austin, Texas 78712, United States; o orcid.org/0000-0002-5880-8649; Email: yuanyue.liu@austin.utexas.edu

Authors

Saerom Yu - Texas Materials Institute and Department of Mechanical Engineering, The University of Texas at Austin, Austin, Texas 78712, United States

Zachary Levell – *Texas Materials Institute and Department of* Mechanical Engineering, The University of Texas at Austin, Austin, Texas 78712, United States

Zhou Jiang - Texas Materials Institute and Department of Mechanical Engineering, The University of Texas at Austin, Austin, Texas 78712, United States

Xunhua Zhao - Texas Materials Institute and Department of Mechanical Engineering, The University of Texas at Austin, Austin, Texas 78712, United States

Complete contact information is available at: https://pubs.acs.org/10.1021/jacs.3c09193

The authors declare no competing financial interest.

ACKNOWLEDGMENTS

This work is supported by the National Science Foundation (Grant Nos. 1900039, 2029442), ACS PRF (60934-DNI6), and the Welch Foundation (Grant No. F-1959-20180324). This work used computational resources at the National Renewable Energy Lab and the Extreme Science and Engineering Discovery Environment (XSEDE) through allocation TG-CHE190065.

REFERENCES

(1) Stephens, I. E. L.; Rossmeisl, J.; Chorkendorff, I. Toward sustainable fuel cells. Science 2016, 354 (6318), 1378-1379.

- (2) Du, L.; Prabhakaran, V.; Xie, X.; Park, S.; Wang, Y.; Shao, Y. Low-PGM and PGM-free catalysts for proton exchange membrane fuel cells: stability challenges and material solutions. Adv. Mater. 2021, 33 (6), No. 1908232.
- (3) Nie, Y.; Li, L.; Wei, Z. Recent advancements in Pt and Pt-free catalysts for oxygen reduction reaction. Chem. Soc. Rev. 2015, 44 (8), 2168-2201.
- (4) Wu, J.; Yang, H. Platinum-based oxygen reduction electrocatalysts. Acc. Chem. Res. 2013, 46 (8), 1848-1857.
- (5) Wang, X. X.; Swihart, M. T.; Wu, G. Achievements, challenges and perspectives on cathode catalysts in proton exchange membrane fuel cells for transportation. Nature Catalysis 2019, 2 (7), 578-589.
- (6) Wu, G.; More, K. L.; Johnston, C. M.; Zelenay, P. Highperformance electrocatalysts for oxygen reduction derived from polyaniline, iron, and cobalt. Science 2011, 332 (6028), 443-447.
- (7) He, Y.; Wu, G. PGM-free oxygen-reduction catalyst development for proton-exchange membrane fuel cells: challenges, solutions, and promises. Accounts of Materials Research 2022, 3 (2), 224-236.
- (8) Shao, M.; Chang, Q.; Dodelet, J.-P.; Chenitz, R. Recent advances in electrocatalysts for oxygen reduction reaction. Chem. Rev. 2016, 116 (6), 3594-3657.
- (9) Dai, L.; Xue, Y.; Qu, L.; Choi, H.-J.; Baek, J.-B. Metal-free catalysts for oxygen reduction reaction. Chem. Rev. 2015, 115 (11), 4823-4892.
- (10) Jasinski, R. A new fuel cell cathode catalyst. Nature 1964, 201 (4925), 1212-1213.
- (11) He, Y.; Liu, S.; Priest, C.; Shi, Q.; Wu, G. Atomically dispersed metal-nitrogen-carbon catalysts for fuel cells: advances in catalyst design, electrode performance, and durability improvement. Chem. Soc. Rev. 2020, 49 (11), 3484-3524.
- (12) Liu, S.; Li, C.; Zachman, M. J.; Zeng, Y.; Yu, H.; Li, B.; Wang, M.; Braaten, J.; Liu, J.; Meyer, H. M.; et al. Atomically dispersed iron sites with a nitrogen-carbon coating as highly active and durable oxygen reduction catalysts for fuel cells. Nature Energy 2022, 7 (7), 652-663.
- (13) Wan, X.; Liu, X.; Li, Y.; Yu, R.; Zheng, L.; Yan, W.; Wang, H.; Xu, M.; Shui, J. Fe-N-C electrocatalyst with dense active sites and efficient mass transport for high-performance proton exchange membrane fuel cells. Nature Catalysis 2019, 2 (3), 259-268.
- (14) Jiao, L.; Li, J.; Richard, L. L.; Sun, Q.; Stracensky, T.; Liu, E.; Sougrati, M. T.; Zhao, Z.; Yang, F.; Zhong, S.; et al. Chemical vapour deposition of Fe-N-C oxygen reduction catalysts with full utilization of dense Fe-N4 sites. Nat. Mater. 2021, 20 (10), 1385-1391.
- (15) Li, J.; Sougrati, M. T.; Zitolo, A.; Ablett, J. M.; Oğuz, I. C.; Mineva, T.; Matanovic, I.; Atanassov, P.; Huang, Y.; Zenyuk, I.; et al. Identification of durable and non-durable FeNx sites in Fe-N-C materials for proton exchange membrane fuel cells. Nature Catalysis 2021, 4 (1), 10-19.
- (16) Mehmood, A.; Gong, M.; Jaouen, F.; Roy, A.; Zitolo, A.; Khan, A.; Sougrati, M.-T.; Primbs, M.; Bonastre, A. M.; Fongalland, D.; et al. High loading of single atomic iron sites in Fe-NC oxygen reduction catalysts for proton exchange membrane fuel cells. Nature Catalysis **2022**, 5 (4), 311–323.
- (17) Ni, L.; Gallenkamp, C.; Wagner, S.; Bill, E.; Krewald, V.; Kramm, U. I. Identification of the Catalytically Dominant Iron Environment in Iron- and Nitrogen-Doped Carbon Catalysts for the Oxygen Reduction Reaction. J. Am. Chem. Soc. 2022, 144 (37), 16827-16840.
- (18) Luo, F.; Roy, A.; Sougrati, M. T.; Khan, A.; Cullen, D. A.; Wang, X.; Primbs, M.; Zitolo, A.; Jaouen, F.; Strasser, P. Structural and Reactivity Effects of Secondary Metal Doping into Iron-Nitrogen-Carbon Catalysts for Oxygen Electroreduction. J. Am. Chem. Soc. **2023**, 145 (27), 14737-14747.
- (19) Zhao, X.; Levell, Z. H.; Yu, S.; Liu, Y. Atomistic understanding of two-dimensional electrocatalysts from first principles. Chem. Rev. **2022**, 122 (12), 10675–10709.
- (20) Zhao, X.; Liu, Y. Origin of selective production of hydrogen peroxide by electrochemical oxygen reduction. J. Am. Chem. Soc. **2021**, 143 (25), 9423–9428.

- (21) Kim, D.; Shi, J.; Liu, Y. Substantial impact of charge on electrochemical reactions of two-dimensional materials. *J. Am. Chem. Soc.* **2018**, *140* (29), 9127–9131.
- (22) Rossmeisl, J.; Skúlason, E.; Björketun, M. E.; Tripkovic, V.; Nørskov, J. K. Modeling the electrified solid–liquid interface. *Chem. Phys. Lett.* **2008**, 466 (1–3), 68–71.
- (23) Chan, K.; Nørskov, J. K. Potential dependence of electrochemical barriers from ab initio calculations. *J. Phys. Chem. Lett.* **2016**, 7 (9), 1686–1690.
- (24) Bonnet, N.; Morishita, T.; Sugino, O.; Otani, M. First-Principles Molecular Dynamics at a Constant Electrode Potential. *Phys. Rev. Lett.* **2012**, *109* (26), No. 266101.
- (25) Surendralal, S.; Todorova, M.; Finnis, M. W.; Neugebauer, J. First-Principles Approach to Model Electrochemical Reactions: Understanding the Fundamental Mechanisms behind Mg Corrosion. *Phys. Rev. Lett.* **2018**, *120* (24), No. 246801.
- (26) Kastlunger, G.; Lindgren, P.; Peterson, A. A. Controlled-Potential Simulation of Elementary Electrochemical Reactions: Proton Discharge on Metal Surfaces. *J. Phys. Chem. C* **2018**, 122 (24), 12771–12781.
- (27) Chen, J.-W.; Zhang, Z.; Yan, H.-M.; Xia, G.-J.; Cao, H.; Wang, Y.-G. Pseudo-adsorption and long-range redox coupling during oxygen reduction reaction on single atom electrocatalyst. *Nat. Commun.* **2022**, *13* (1), 1734.
- (28) Sundararaman, R.; Vigil-Fowler, D.; Schwarz, K. Improving the Accuracy of Atomistic Simulations of the Electrochemical Interface. *Chem. Rev.* **2022**, *122* (12), 10651–10674.
- (29) Hutchison, P.; Rice, P. S.; Warburton, R. E.; Raugei, S.; Hammes-Schiffer, S. Multilevel computational studies reveal the importance of axial ligand for oxygen reduction reaction on Fe-N-C materials. J. Am. Chem. Soc. 2022, 144 (36), 16524–16534.
- (30) Xia, D.; Yang, X.; Xie, L.; Wei, Y.; Jiang, W.; Dou, M.; Li, X.; Li, J.; Gan, L.; Kang, F. Direct growth of carbon nanotubes doped with single atomic Fe—N4 active sites and neighboring graphitic nitrogen for efficient and stable oxygen reduction electrocatalysis. *Adv. Funct. Mater.* **2019**, 29 (49), No. 1906174.
- (31) Xiao, M.; Xing, Z.; Jin, Z.; Liu, C.; Ge, J.; Zhu, J.; Wang, Y.; Zhao, X.; Chen, Z. Preferentially engineering FeN4 edge sites onto graphitic nanosheets for highly active and durable oxygen electrocatalysis in rechargeable Zn—air batteries. *Adv. Mater.* **2020**, 32 (49), No. 2004900.
- (32) Wan, H.; Jensen, A. W.; Escudero-Escribano, M.; Rossmeisl, J. Insights in the oxygen reduction reaction: from metallic electrocatalysts to diporphyrins. *ACS Catal.* **2020**, *10* (11), 5979–5989.
- (33) Hu, X.; Chen, S.; Chen, L.; Tian, Y.; Yao, S.; Lu, Z.; Zhang, X.; Zhou, Z. What is the real origin of the activity of Fe-N-C electrocatalysts in the o2 reduction reaction? critical roles of coordinating pyrrolic n and axially adsorbing species. *J. Am. Chem. Soc.* 2022, 144 (39), 18144–18152.
- (34) Wang, Y.; Tang, Y.-J.; Zhou, K. Self-adjusting activity induced by intrinsic reaction intermediate in Fe–N–C single-atom catalysts. *J. Am. Chem. Soc.* **2019**, *141* (36), 14115–14119.
- (35) Yan, X.; Liu, K.; Wang, T.; You, Y.; Liu, J.; Wang, P.; Pan, X.; Wang, G.; Luo, J.; Zhu, J. Atomic interpretation of high activity on transition metal and nitrogen-doped carbon nanofibers for catalyzing oxygen reduction. *Journal of Materials Chemistry A* **2017**, 5 (7), 3336–3345.
- (36) Zheng, T.; Wang, J.; Xia, Z.; Wang, G.; Duan, Z. Spin-dependent active centers in Fe-N-C oxygen reduction catalysts revealed by constant-potential density functional theory. *Journal of Materials Chemistry A* **2023**, *11* (36), 19360–19373.
- (37) Kresse, G.; Furthmüller, J. Efficiency of ab-initio total energy calculations for metals and semiconductors using a plane-wave basis set. *Computational materials science* **1996**, 6 (1), 15–50.
- (38) Kresse, G.; Hafner, J. Ab initio molecular dynamics for liquid metals. *Phys. Rev. B* **1993**, *47* (1), 558.
- (39) Mathew, K.; Sundararaman, R.; Letchworth-Weaver, K.; Arias, T. A.; Hennig, R. G. Implicit solvation model for density-functional

- study of nanocrystal surfaces and reaction pathways. J. Chem. Phys. 2014, 140 (8), No. 084106.
- (40) Mathew, K.; Kolluru, V. S. C.; Mula, S.; Steinmann, S. N.; Hennig, R. G. Implicit self-consistent electrolyte model in plane-wave density-functional theory. *J. Chem. Phys.* **2019**, *151* (23), No. 234101.
- (41) Jarzynski, C. Nonequilibrium equality for free energy differences. *Phys. Rev. Lett.* **1997**, 78 (14), 2690.
- (42) Carter, E. A.; Ciccotti, G.; Hynes, J. T.; Kapral, R. Constrained reaction coordinate dynamics for the simulation of rare events. *Chem. Phys. Lett.* **1989**, *156* (5), 472–477.
- (43) Sprik, M.; Ciccotti, G. Free energy from constrained molecular dynamics. J. Chem. Phys. 1998, 109 (18), 7737–7744.
- (44) Zhang, H.; Hwang, S.; Wang, M.; Feng, Z.; Karakalos, S.; Luo, L.; Qiao, Z.; Xie, X.; Wang, C.; Su, D. Single atomic iron catalysts for oxygen reduction in acidic media: particle size control and thermal activation. *J. Am. Chem. Soc.* **2017**, *139* (40), 14143–14149.
- (45) Li, J.; Zhang, H.; Samarakoon, W.; Shan, W.; Cullen, D. A.; Karakalos, S.; Chen, M.; Gu, D.; More, K. L.; Wang, G. Thermally driven structure and performance evolution of atomically dispersed FeN4 sites for oxygen reduction. *Angew. Chem., Int. Ed.* **2019**, *58* (52), 18971–18980.